JCTC Journal of Chemical Theory and Computation

pubs.acs.org/JCTC Article

Investigating a Combined Stochastic Nucleation and Molecular Dynamics-Based Equilibration Approach for Constructing Large-Scale Polycrystalline Films

K. Sebastian Schellhammer, Gianaurelio Cuniberti, and Frank Ortmann*

Cite This: J. Chem. Theory Comput. 2021, 17, 1266−1275 Read Online

ACCESS | Metrics & More | Article Recommendations | Supporting Information

ABSTRACT: The morphology of small-molecule organic semiconducting materials can vary from single crystals via polycrystalline films with varying grain sizes to amorphous structures, depending on the process conditions. This structural variety affects the electronic properties and, thus, the performance of organic electronic devices. A nucleation-equilibration approach is investigated, whose focus is on the construction of morphologies with controlled variations in the average grain size. Its computational requirements are low because nucleation is purely based on geometrical considerations, thus allowing the construction of model systems of experimentally relevant sizes. Its application is demonstrated for C_{60} and pentacene by generating single-component films that vary from amorphous to crystalline structures. It is further generalized to two-component films and applied to C_{60}: pentacene blends as well as dilute n-doped C_{60} structures. When combined with electronic structure calculations in the future, the nucleation-equilibration approach can offer insights into the impact of polycrystallinity on electronic and charge-transport properties in the absence of any knowledge about the growth mechanism and for a broad set of systems.

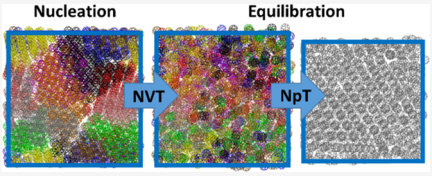

1. INTRODUCTION

Organic semiconductors are known to exhibit a large variety of morphologies, which differ in their local molecular arrangements. For example, the morphology of pentacene can be varied from micron-sized single crystals,[1,2] via polycrystalline phases, with crystalline grains in the 10−100 nm range,[3−5] to amorphous phases.[6,7] Such variations affect the local electronic properties through variations in electronic coupling between molecular orbitals and local variations in the dielectric polarization effects. Such local features can substantially influence global properties. For instance, they can affect the charge carrier mobility by orders of magnitude.[8−13] Consequently, the optimization of organic electronic devices calls for a detailed understanding of the complex relationship between material morphology, electronic properties, and macroscopic device performance.

In contrast to the rich spectrum of experimentally accessible structures, theoretical charge-transport studies have focused mostly on the two limiting scenarios of either perfectly crystalline or completely amorphous phases. The limit of highly ordered structures is covered by different approaches that use experimental crystal-structure information,[13−20] while an increasing amount of disorder can be added by molecular dynamics (MD) simulations or disorder models.[15,17,21] On the other hand, amorphous structures were created and studied by simulated annealing or stochastic approaches.[22−24]

More challenging simulation targets are the partly disordered systems (with some long-range order) and the description of the influence of grain boundaries. Park et al. developed an effective model for the treatment of grain boundaries in charge-transport simulations in polycrystalline thin films.[12] Their simulations are based on crystalline structures with polycrystallinity being adjusted according to the results from atomic force microscopy experiments. Kwiatkowski et al. simulated the physical vapor deposition process to reproduce the experimental trends of growing grain sizes while increasing the substrate temperature.[25] Still, in their approach, the accessible grain sizes are significantly below experimentally relevant length scales, and large computational resources are a bottleneck for further upscaling the treatable sample sizes. Recently, a combination of probabilistic growth and equilibration simulations has been used for the simulation of charge transport in two-dimensional (2D) polycrystalline TIPS−pentacene structures.[26]

In this study, we investigate a scale bridging nucleation-equilibration approach to construct three-dimensional (3D) models of polycrystalline films with varying degrees of order and molecules of varying shapes, which is demonstrated for pure C_{60} and pure pentacene model structures as well as for C_{60}: pentacene blends and n-doped C_{60} films. Herein, a nucleation algorithm generates large structures (with more

Received: November 15, 2020
Published: January 12, 2021

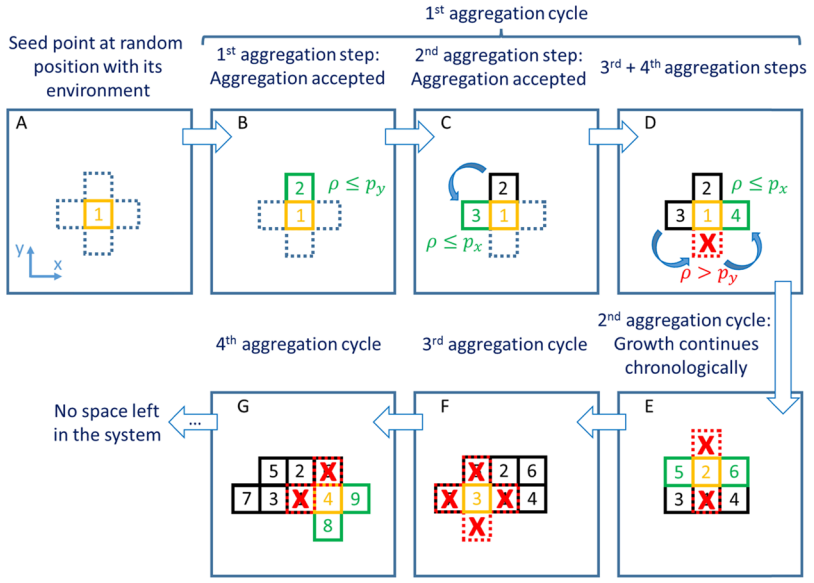

Figure 1. Schematic illustration of the workflow of the nucleation algorithm in 2D. (B–D) Aggregation cycle for site 1 (yellow box in A–D) leads to the attachment of neighbor sites 2 to 4 to the growing cluster. (E) Second aggregation cycle leads to the addition of sites 5 and 6 to site 2 (yellow box in E). (F) Within the third aggregation cycle, no further molecules are attached to site 3 (yellow box in F) because of overlapping molecules or an unsatisfied aggregation criterion. (G) Fourth aggregation cycle leads to the addition of sites 8 and 9 to site 4 (yellow box in G).

than 1,000,000 molecules) with varying average grain sizes using an underlying predefined lattice model and a purely geometrical aggregation model. These structures are equilibrated at ambient conditions by performing force-field-based MD simulations. The structural orders in the created polycrystalline samples can be controlled by a small set of input parameters, which makes the approach widely applicable. The structures exhibit grains of controllable average size that are connected by small diffuse regions. The richness of the structures that are accessible with the algorithm is an essential factor toward the systematic theoretical studies of morphology effects on the electronic structure and transport properties of organic semiconductors.

2. METHODOLOGY

2.1. Nucleation Algorithm. In the following, the generic form of the nucleation algorithm is presented for the growth of a single grain of a polycrystalline sample; while in practice, multiple grains grow simultaneously, ensuring controllable average grain sizes. More specific aspects of the algorithm for spherical and nonspherical molecules as well as blended structures are discussed in the following sections. The workflow is schematically depicted in Figure 1, which considers the case of 2D grain growth. 2D growth has previously been employed for a charge-transport study.[26] Here, a 2D geometry is only used for illustration purposes, while the approach is employed for 3D samples throughout this study. The pseudocode of the algorithm is presented in Scheme 1.

The growth of a single grain can be imagined as a stepwise construction of a single crystal by adding more molecules in the crystal lattice up to the point where neighboring grains contact each other. The lattice vectors and the molecular basis of the chosen crystal structure in the grains (we consider multiple molecules per primitive unit cell) are used to define the environment of each molecule in the lattice. The considered molecule is indicated in all the subfigures of Figure 1 by a yellow box. The environment of a molecule is the smallest set of neighboring molecules in all the directions that

Scheme 1. Pseudocode of the Nucleation Algorithm without Periodic Boundary Conditions

```
Sub nucleation(l, p_i, r_i)
  j = 1
  N = 1
  COM_j = [rand · l; rand · l; rand · l]
  While j ≤ N
    For i = 1 to N_neigh
      If overlap criterion is true and rand < p_i then
        N+= 1
        set molecule at COM_N = COM_j + r_i
      End If
    Next i
    j+= 1
  End While
End Sub
```

is sufficient to construct the grain iteratively. N_{neigh} is the number of elements in this set. In addition to the information about the positions of the neighboring molecules with respect to the considered molecule, $\boldsymbol{r}_i$, we track the molecule index inside the unit cell in case there is more than one. In the example presented in Figure 1, the environment of each molecule consists of $N_{neigh} = 4$ nearest neighbors at positions $(\pm a,0,0)$ and $(0, \pm a,0)$ with a being the nearest-neighbor distance (dashed boxes in Figure 1A). For the convenience of presentation, all these molecules have the same orientation, that is, the molecular basis of the crystal structure in this example consists of only one molecule.

In the first step of the nucleation algorithm, the seed point of a given grain is placed at a random position (Figure 1A, central yellow box). The orientation of the grain is determined randomly. For illustration purposes, the grain is aligned with the coordinate axes shown in Figure 1. Next, the first aggregation cycle for the seed molecule starts by systematically controlling the aggregation of additional molecules in its environment. Each so-attached molecule will be the center of

https://dx.doi.org/10.1021/acs.jctc.0c01196
J. Chem. Theory Comput. 2021, 17, 1266–1275

another aggregation cycle such that all the molecules will be subsequently processed. An aggregation cycle consists of N_{neigh} aggregation steps. In the example depicted in Figure 1, an aggregation cycle always starts at $(0,+a,0)$ and analyzes all the elements of the environment anticlockwise.

In an aggregation step, two criteria control the possible attachment of a molecule in the environment, namely, (1) the overlap criterion and (2) the aggregation criterion. The overlap criterion excludes molecular overlap (i.e., too close molecules) within the same grain and between different grains. This is necessary to avoid doubly occupied sites or the overlap of molecules within grains and of neighboring grains. The aggregation criterion is introduced additionally to allow for the variation of grain shapes and the indirect consideration of aggregation energetics. It is based on aggregation probability p_i ($i = 1...N_{neigh}$), which is defined initially for each element of the environment. The aggregation criterion is satisfied for $\rho \leq p_i$ with ρ being a uniformly distributed random number. The choice of values for the p_i can be used to control the growth in different directions. If both criteria are satisfied for a molecule from the environment, it is added to the aggregate at its position. Otherwise, the position is left empty but not blocked for aggregation in later aggregation cycles. Both the cases terminate the aggregation step, and one proceeds to the next step that considers the next molecule from the environment.

In the example presented in Figure 1, the aggregation criterion is effectively switched off in the x direction by choosing $p_x = 1$, that is, growth is always allowed if the overlap criterion is satisfied. The growth in the y direction is chosen to be energetically less favorable than that in the x direction using $p_y < 1$. In Figure 1B, the first aggregation step of the first aggregation cycle is shown. Both criteria are satisfied at $(0, +a,0)$, leading to the acceptance of the nearest neighbor and the placement of the second molecule in the grain. In the next aggregation step, the position $(-a,0,0)$ is tested for aggregation (cf. Figure 1C). As both criteria are satisfied again, aggregation is accepted, and the third molecule is placed. Figure 1D shows the last two aggregation steps of the first aggregation cycle. At $(0,-a,0)$, aggregation is rejected because the aggregation criterion is not satisfied ($\rho > p_y$). In contrast, the fourth molecule in the grain is attached at $(+a,0,0)$ because both criteria are fulfilled. The first aggregation cycle finishes with all the sites of the environment checked.

The growth of the grain continues chronologically: The next aggregation cycle is run for the environment of the second molecule placed in the grain (cf. Figure 1E). The growth of grains ends when the aggregation cycles are finished for all the molecules of the grain. For the construction of polycrystalline structures, multiple grains grow simultaneously with one molecule being potentially aggregated at each grain per nucleation step. Because of this systematic aggregation process, each molecule is associated with a certain grain. This information is connected with the molecular ID number, which allows the tracking of the molecular transitions between the grains at the grain boundaries during equilibration. The nucleation algorithm ends when all the aggregation cycles are finished for all the grains in the system.

2.2. Equilibration. The aim of structure equilibration using MD simulations is the removal of potential artifacts from the initial structures constructed using the abovementioned nucleation algorithm and the convergence of the structures toward the desired thermodynamic conditions. For this purpose, we apply and compare two types of equilibration modes: (1) the NpT mode and (2) the NVT + NpT mode. They are compared below for prototypical systems. In the first case, the structures from the nucleation algorithm are directly simulated in an NpT ensemble (300 K, 1 atm) for 10 ns by a Nosé−Hoover thermostat with a coupling constant of 0.4 ps and a Berendsen barostat with a coupling constant of 4 ps and a compressibility of $4.5 \cdot 10^{-5}$ bar^{-1}.[27−29] In the NVT + NpT mode, the initial structure is first simulated in an NVT ensemble for 100 ps using again a Nosé−Hoover thermostat. Afterward, the structure is simulated in an NpT ensemble with the same parameters as in the NpT mode. The corresponding MD simulations are performed using the GROMACS software package.[30−32] All atomic charges are set to zero for a reduced computational effort in order to maximize the possible sample sizes. The benchmark calculations including atomic charges did not affect the equilibrated structures significantly. Van der Waals interactions are included using a particle-mesh Ewald approach in combination with a cutoff radius of 1 nm. The van der Waals potential is shifted by a constant such that it is zero at the cutoff. All MD simulations are performed using a time step of 1 fs.

3. APPLICATIONS FOR SPHERICAL MOLECULES: C_{60}

In this section, we generate samples of polycrystalline C_{60} at ambient conditions that vary systematically in their average grain size, as a representative case for spherical (and similarly shaped) molecules. We define the grain size in terms of the average number of molecules per grain $\eta = \frac{N}{N_{grains}}$ (with N as the total number of molecules in the sample) as a measure for the degree of structural order in the sample. This definition is extended to the cases $\eta = 1$ (amorphous phase) and $\eta = \infty$ (single crystal without grain boundaries or defects). Periodic boundary conditions in the three Cartesian directions are applied for all the structures.

3.1. Nucleation Algorithm. The basic input information for the algorithm is as follows: (i) the size of the to-be-generated sample, which is given by the size of the cubic box l, (ii) the desired grain size η, which is specified by the number of grains N_{grains} that are placed in the box, (iii) the environment of each molecule (see the definition above), (iv) the overlap criterion, and (v) the aggregation criterion. The environment of each molecule is defined based on the face-centered cubic phase of C_{60} with a lattice constant of $a = 1.417$ nm, which has been observed for temperatures above 249 K.[33] Each molecule has 12 nearest neighbors at a distance of $r_{crys} = 1$ nm. The orientation of the molecules is chosen randomly as they are rotationally disordered for temperatures above 260 K.[34]

The aggregation criterion is deactivated ($p_i = 1$ for all i) because aggregation is expected to occur isotropically for C_{60}. Consequently, aggregation occurs always if the overlap criterion is satisfied. The overlap criterion is defined by the spherical shape of C_{60} as follows. The molecules are represented by the position of their center of mass (COM) and a spherical interaction shell described by an interaction radius r_{int}. We require that no other COMs can be placed in this interaction shell.[23] Hence, the overlap criterion in an aggregation step is not satisfied if the COM of the candidate is in any of the existing interaction spheres. This would lead to the rejection of the candidate. A reasonable choice is to use $r_{int} = r_{crys}$, which also reduces the number of internal parameters.

The application of the nucleation algorithm is illustrated in Figure 2A−E for a small prototypical structure with $N_{grains} = 10$

https://dx.doi.org/10.1021/acs.jctc.0c01196
J. Chem. Theory Comput. 2021, 17, 1266−1275

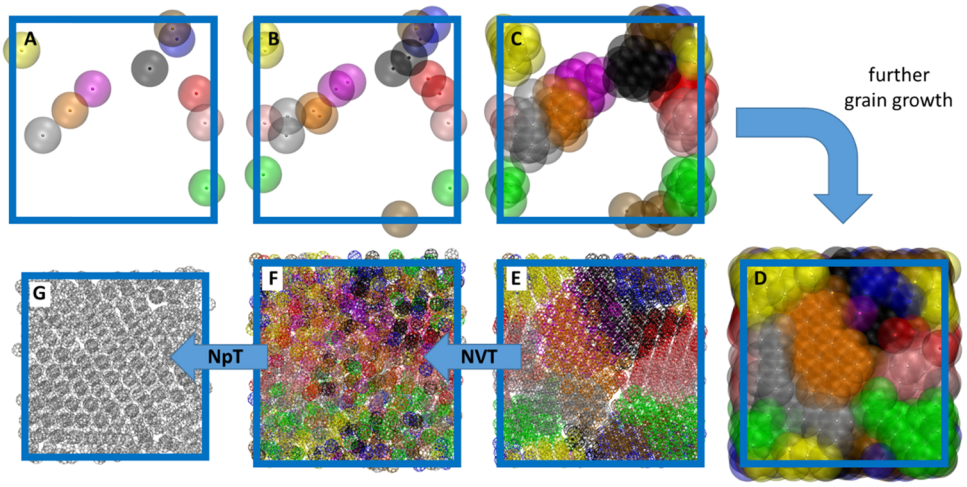

Figure 2. Workflow of the nucleation-equilibration algorithm for spherical molecules demonstrated for C_{60} with $N \approx 1000$ and $\eta = 100$.

and $l = 10$ nm. First, N_{grains} seed points are placed at random positions. It should be noted that the seed points also have to satisfy the overlap criterion (Figure 2A). In the first aggregation step, each grain grows simultaneously by one molecule (cf. Figure 2B). The figure also shows the random orientation of the individual grains. Then, the grains grow further stepwise. In Figure 2C, the first aggregation cycle is finished with all the grain seeds having 12 nearest neighbors (the overlap criterion was satisfied for all the molecules of the environment of each of the seed molecules). In the next aggregation cycle, aggregation continues at the second molecule of each individual grain. The grains stop growing if the aggregation cycle of the last molecule in the grain is finished. The algorithm stops if this is satisfied for all the grains (cf. Figure 2D). In the last step of the nucleation algorithm, the molecules are placed at the COM points with random orientation, as shown in Figure 2E.

The nucleation algorithm presented here is based solely on geometrical conditions, not taking the energetics like surface energies or the impact by the substrate explicitly into account. It is to be noted that the stepwise environment-based growth mode mimics an isotropic grain growth of C_{60} via low-energy grain surfaces, although the final shape of the grains is governed by the initial random placement of the seeds. This leads to compact grain structures at a low computational cost because the simulation time scales linearly with the total number of molecules in the system N. Instead of mimicking a number of variants of grain growth more specifically, the nucleation algorithm aims at constructing prototypical film samples with tunable parameter η for systematic theoretical investigations, which is particularly useful in the absence of experimental knowledge about the growth.

We use the nucleation algorithm for the construction of C_{60} structures with gradually increasing average grain sizes η, as depicted in Figure 3A–C for a box size of $l = 42$ nm and approximately 100,000 molecules. Different grain sizes can be identified visually. To better quantify the degree of short-range and long-range orders of the generated samples, we calculate the radial pair-distribution function (PDF) based on the position of the COM of the molecules shown in Figure 4A. While for $\eta = 200$, we find strong positional correlations only within 5 nm, with an increasing average grain size; the correlation length systematically increases to 9 nm for $\eta = 2000$ and more than 15 nm for $\eta = 20{,}000$. This further quantifies

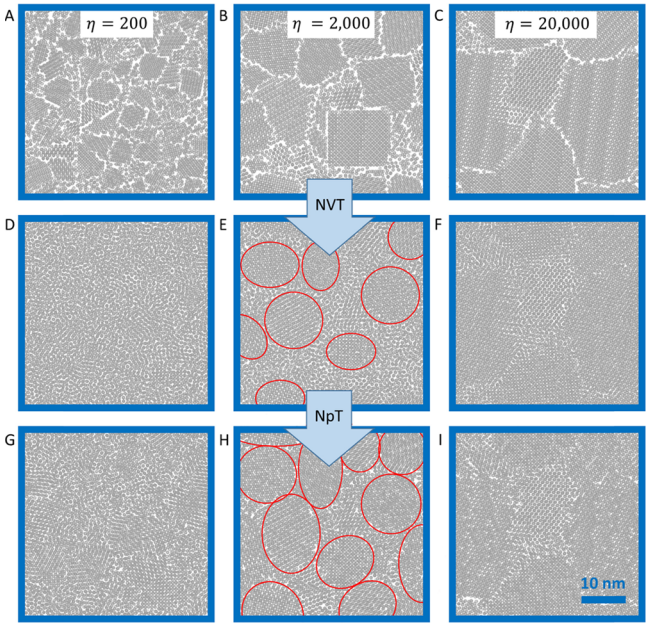

Figure 3. Prototypical C_{60} structures created by the nucleation algorithm (A–C), structures after the first equilibration step in the NVT ensemble (D-F), and structures after the second equilibration step in the NpT ensemble (G–I). For reasons of visibility, only the first layers are depicted in the viewing direction. System sizes are approximately 42×42×42 nm^3. To conserve the structural order during equilibration for $\eta = 200$, r_{int} and r_{crys} are reduced to 0.94 nm (see the main text).

the gradually increasing long-range order with increasing η. Therefore, the degree of order can be easily controlled by a variation of the input parameters.

The density of molecules is another quantity to characterize the structures and is depicted in Figure 5 (red circles). With the increasing grain size, it increases steadily toward the density of the disorder-free crystalline structure ($\eta = \infty$). For $\eta < 5000$, a strong decrease in the density can be observed, which appears to be slightly artificial especially when considering the spherical shape of C_{60}. We also observe that the grains are not sufficiently connected. Indeed, the grain boundaries already appear as relatively large cracks in Figure 3A–C. The occurrence of such gaps between the grains is a

https://dx.doi.org/10.1021/acs.jctc.0c01196
J. Chem. Theory Comput. 2021, 17, 1266–1275

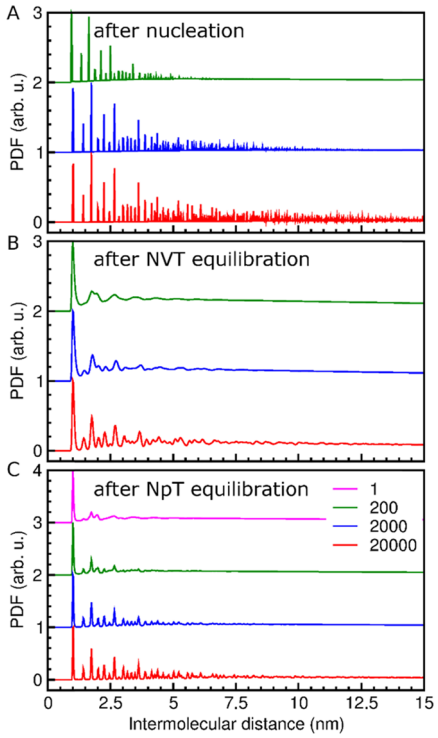

Figure 4. Normalized radial PDFs of C_{60} structures at different stages of the nucleation-equilibration approach. (A) Initial structures created by the nucleation algorithm. (B) After the first equilibration step in the NVT ensemble. (C) After the second equilibration step in the NpT ensemble. To conserve the structural order during equilibration for η = 200, r_{int} and r_{crys} are reduced to 0.94 nm. Graphs are shifted along the y axis for improved visibility and normalized with respect to their maximum.

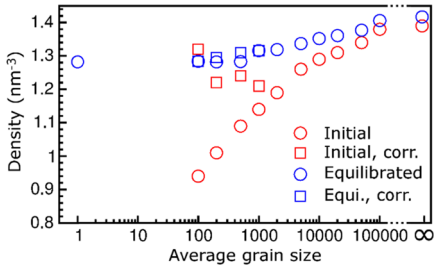

Figure 5. Molecular density of C_{60} structures versus average grain size of the initial constructed grains from the nucleation algorithm (red symbols) and after full equilibration with the two-step approach (blue symbols). Circles correspond to $r_{int} = r_{crys}$ = 1 nm. Squares correspond to the application of the correction step with $r_{int} = r_{crys} < 1$ nm.

general signature of the nucleation algorithm, which can be cured by performing equilibration.

3.2. Equilibration. MD simulations are performed to equilibrate the structures at ambient conditions as well as to remove artificial features from the nucleation algorithm in the structures, such as artificial grain connections. As MD simulations can potentially randomize the constructed structures completely, the challenge of the equilibration step is to conserve the degree of polycrystallinity that was chosen initially. We monitor the local and global order with the radial PDF shown in Figure 4.

For C_{60}, the Martini force field based on Girifalco's van der Waals parameters is known to accurately reproduce its experimental lattice constant.[35−37] This finding is rediscovered by us for a perfectly ordered supercell comprising 4000 molecules. This single-crystalline structure is referred to as $\eta = \infty$ in the following. It exhibits an infinite long-range order and a molecular density of 1.41 nm^{-3}.

The two equilibration modes are tested for the constructed polycrystalline C_{60} structures. Simulations in the NpT mode lead to a strong expansion of the structures by several nanometers in the first picoseconds of the simulations. The expansion is accompanied by a loss of the initial polycrystalline order. This behavior can be described as melting of the structures. In the following nanoseconds, the systems condense back to compact morphologies reminiscent of simulated annealing procedures. The obtained structures show the lowest structural order and are referred to as η = 1 in Figure 4C because they are dominated by amorphous regions (despite singular minigrains of ∼100 molecules). The structures show almost an identical density of 1.28 nm^{-3} and a radial PDF (Figure 4C) independent of the initial value of η. Consequently, the NpT mode does not conserve the desired polycrystallinity.

In contrast, using the NVT + NpT equilibration mode with intermediate equilibration under NVT ensemble conditions, complete melting is avoided. A rather short simulation time of 100 ps leads to a more controlled partial melting process of the structures, as shown in Figure 3D−F. The grains expand in the NVT simulations. However, because the total volume is constant, this is at the expense of the low-density grain-boundary regions. While the initial structures appear unconnected at the grain boundaries (Figure 3A−C), after this expansion, the grain boundaries can be identified as diffuse areas between the grains (grains are highlighted by red ellipses in Figure 3E). Simultaneously, the order in the grains is somewhat reduced, causing the broadening of the short-range features in the PDFs (cf. Figure 4B). Still, the structures can be described as polycrystalline. In the second equilibration step, under NpT ensemble conditions, the structures are compressed. After the simulation time of 10 ns, the volume of the structures is converged. In contrast to the initial structures with loosely connected grains with sharp surfaces and edges, the grain boundaries of the final structures are rather blurred and continuous (Figure 3G−I). These amorphous areas of the grain boundaries are also much narrower (thickness of ∼3 nm) than in the morphologies after the first equilibration step (Figure 3D−F). This is accompanied by an increasing order in the grains. The compression of the structures including these structural changes leads to an increase in the molecular density, as shown in Figure 5 (blue circles). While a strong decrease in the density with a reduced average grain size was observed for the initial structures (red circles), a much shallower decrease was observed for the fully equilibrated structures. It is to be noted that the simulations of structures with the same intended average grain size η but constructed using a different seed for the random number generator in the nucleation algorithm lead to equilibrated structures with indistinguishable PDF and density after equilibration.

When carefully analyzing the molecular density, all the structures created with $\eta \leq 500$ reveal the same density of 1.28 nm^{-3}, which appears slightly artificial. This value was already observed in simulations in the NpT equilibration mode for the almost-amorphous structures. Indeed, the analysis of the PDF shows the same relatively featureless behavior without a considerable long-range order, as shown for η = 1 in Figure 4C.

https://dx.doi.org/10.1021/acs.jctc.0c01196
J. Chem. Theory Comput. 2021, 17, 1266−1275

We trace back this loss of order in these structures to the artificially low densities of the initial structures (below 1.1 nm^{-3} for $\eta \leq 500$ in Figure 5). To allow for the construction of structures also for small average grain sizes below $\eta \leq 500$, we propose a simple correction step. We reduce the intermolecular distances r_{crys} and r_{int} below the distance that is found in the crystal geometry by choosing a scaling parameter s (with $s < 1$) such that the densities of the initial structures are increased. In Figure S1 in the Supporting Information (SI), the PDF and the density are presented under the variation of s for $\eta = 100$ and $N \approx 10{,}000$. With the densities of the initial structures above 1.2 nm^{-3}, the structural order is improved, as can be seen in the PDF, and smaller average grain sizes are accessible. For larger structures with $N \approx 100{,}000$, the application of this correction step leads to the conservation of the structural order for systems only for $\eta \geq 200$, whereas below this value, more complex mixed morphologies (e.g., with locally varying η) can occur. Consequently, larger structures with homogeneous crystallinity can be simulated for $\eta \geq 200$.

The application of the correction step leads to slightly increased densities of the equilibrated structures (Figure 5, blue squares) and a continuously increasing density with η over the entire range of values considered here. We also note that the resulting variation in the density between the equilibrated amorphous and perfectly crystalline structures is rather small because of the relatively dense packing of spherical molecules achieved even in the most disordered case.

4. APPLICATIONS FOR NONSPHERICAL MOLECULES: PENTACENE

4.1. Nucleation Algorithm. In addition to the application to spherical molecules, the nucleation algorithm can be applied to nonspherical molecules, which we demonstrate for pentacene based on grains with the Holmes crystal structure (cf. Figure S2).[38] Here, the environment of each molecule comprises eight neighbors with two different orientations: four have an orientation that is equal to the one of the molecules considered (at positions indicated by $(\pm a,0,0)$ and $(0,0,\pm c)$) and four have a different orientation (at positions $(\pm a/2,\pm b/2,0)$).

The overlap criterion can be implemented for nonspherical molecules by defining critical interatomic distances between neighboring molecules that depend on the atom types. The application of the overlap criterion means that aggregation is excluded if any pair of atoms from different molecules would be too close (below the minimum distance d). For pentacene, $d_{CC} = 2.8$ Å, $d_{CH} = 1.4$ Å, and $d_{HH} = 1.1$ Å yield compact structures.

The aggregation criterion is inspired by the energetics in the Holmes crystal structure. Because of strong intermolecular interactions along the a-stacking direction, p_a is set to 1. This implies that aggregation along this direction is always allowed if the overlap criterion is satisfied. Grain growth along the $a-b$ direction appears energetically less favorable, which is considered by $p_{ab} = 0.25$. Growth along the c direction is energetically the most unfavorable, which is taken into account using $p_c = 0.1$. Instead of the probabilities used here, values can also be provided after analyzing the interaction energies, which, however, is not in the scope of the present work. The variation of these probabilities can modify the grain shapes; however, substantial deviations from low-aspect-ratio grains are limited by the positions of the initial seeds and cannot be identified for the system sizes analyzed here.

For the case of C_{60}, the scaling factor s was introduced that slightly shortened the intermolecular distances in order to conserve the desired structural order after equilibration also for small average grain sizes. This is used for pentacene as well. Without this correction, the decrease in the molecular density of the initial structural guesses created by the nucleation algorithm would be even more pronounced for pentacene than for C_{60}, which would further impede the conservation of the polycrystalline order in the equilibration. As such a correction step does not artificially influence structures with intermediate and large average grain sizes, it is applied for all the structures independent of the targeted average grain size. In the following, we use $s = 0.94$ for pentacene along all the crystal directions.

Using the above specifications, the nucleation algorithm provides pentacene structures with gradually increasing average grain sizes η, which is demonstrated for $N \approx 200{,}000$ in Figure 6A–C. We observe that similarly to C_{60}, the structures

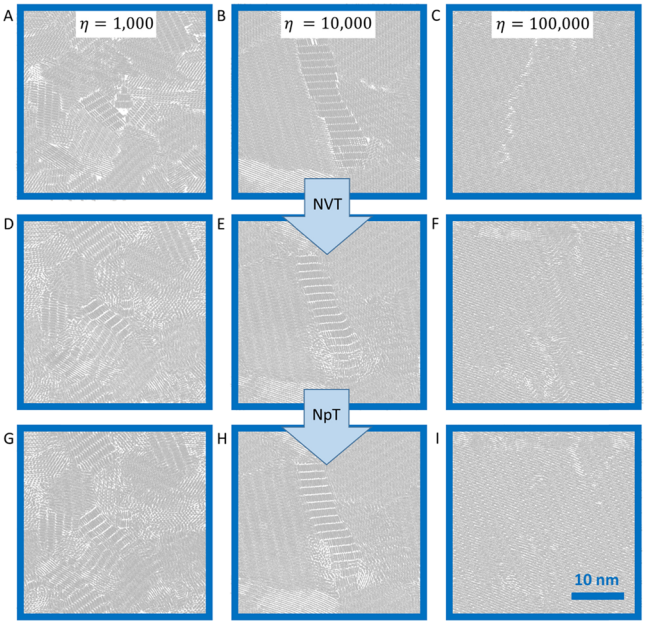

Figure 6. Prototypical pentacene structures created by the nucleation algorithm (A–C), after the first equilibration step in the NVT ensemble (D–F) and after the second equilibration step in the NpT ensemble (G–I). For reasons of visibility, only the first layers are depicted in the viewing direction. System sizes are approximately 35 × 35 × 35 nm^3.

generated in the nucleation algorithm suffer from weakly connected grains (artificial grain boundaries), which will be smoothened during equilibration. Regarding the performance of the nucleation algorithm for nonspherical molecules, we note that it requires slightly increased simulation times because of the more complex implementation of the overlap criterion, showing slightly superlinear scaling on the order of $N^{1.4}$ for the sample sizes considered here. However, it is worth emphasizing that also for nonspherical molecules, the approach maintains its great simplicity, and only crystal-structure information and empirical aggregation probabilities are employed, making it applicable for a large set of molecules.

4.2. Equilibration. The OPLS-aa force field is used for the equilibration of the polycrystalline pentacene structures.[39,40] The accuracy of the force field is checked by applying the NpT

https://dx.doi.org/10.1021/acs.jctc.0c01196
J. Chem. Theory Comput. 2021, 17, 1266–1275

equilibration mode to a crystalline pentacene structure. We find that the experimental lattice vectors are reproduced with an overestimation of the volume of the unit cell by 4%. Introducing additional atomic charges in the simulations does not lead to a significant improvement, but it strongly increases the computational effort; therefore, it was not considered further.

As performed for C_{60}, the NpT equilibration mode and the NVT + NpT mode are applied to the initial structures. Direct equilibration in the NpT ensemble leads to the complete melting of the polycrystalline samples. Different from the observations made for C_{60}, all the final structures reveal no long-range order; thus, they can be described as fully amorphous.

In contrast, when applying a NVT run for 100 ps first, as in the NVT + NpT equilibration mode, the grain boundaries change from sharp edges to blurred intergrain regions because of slight structural melting (cf. Figure 6D−F). However, the grains remain clearly visible. In the second equilibration step, the structural order is recovered, as shown in Figure 6G−I, with a smaller deviation of the molecular COMs from the original lattice points. The structural order within the grains resembles the Holmes crystal structure, as indicated by the PDFs that are depicted in Figure S3 in the Supporting Information. The molecular density of the final equilibrated structures shows a continuous dependence on η (from amorphous to single crystal), as depicted in Figure 7. It is

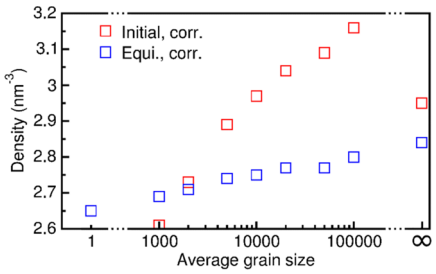

Figure 7. Density of the pentacene structures versus average grain size of the initial constructed grains from the nucleation algorithm (red symbols) and after full equilibration with the two-step approach (blue symbols).

worth mentioning that for large grain sizes, isolated structural defects are possibly induced by the equilibration, as shown in Figure 6I. These features do not appear unrealistic according to experimental studies.[41] Consequently, also for pentacene, the nucleation algorithm constructs samples of the desired structural order, and the NVT + NpT equilibration removes artifacts such as broad gaps between grains while widely conserving the desired degree of polycrystallinity. For the equilibrated structures presented within this study, the diffuse area between the grains is relatively narrow. On the other hand, by decreasing the density of the initial structures using values for s above 1, the range of these amorphous grain-boundary areas could be increased. The impact of the size of the grain boundaries appears interesting for future studies, especially in combination with an analysis of the effects of polycrystallinity on the electronic structure and charge transport.

5. POLYCRYSTALLINE PENTACENE:C_{60} BLENDS

After the abovementioned single-component systems, we discuss the extension of the nucleation-equilibration approach toward mixed structures, which is demonstrated for prototypical pentacene:C_{60} blends in which both the compounds form separate crystalline grains. In the initial step, the grain seeds are randomly placed for C_{60} as well as for pentacene. In the following, for all the grains, aggregation is tested simultaneously using one molecule per nucleation step. For pentacene, the nucleation algorithm can be used as described in Section 4. In contrast to pure C_{60} phases reported in Section 3, the overlap criterion needs to be redefined for C_{60} to reliably exclude any overlap between the C_{60} and pentacene molecules. We use the same approach as that introduced for nonspherical molecules by defining minimum interatomic distances between the neighboring molecules depending on the atom types. For pentacene and C_{60}, d_{CC} = 2.5 Å and d_{HH} = 1.2 Å are used. Two C-H distances are used for different molecular species: $d_{CH}^{C_{60}-Pen}$ = 2.0 Å and $d_{CH}^{C_{Pen}-Pen}$ = 1.5 Å to account for the different molecular shapes.

These configurations yield compact initial structures, as representatively shown in Figure 8A. The characteristic broken

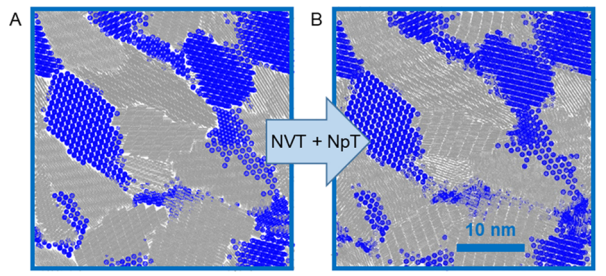

Figure 8. Prototypical C_{60}:pentacene blend structures created by the nucleation algorithm (A) and after full two-step equilibration (B). The mixing ratio is 1:2 with η = 4000 for both molecular species. For clarity, only the first layers are depicted in the viewing direction. System sizes are approximately 38 × 38 × 38 nm^3. The C_{60} molecules are colored blue, and the pentacene molecules are colored gray.

structures at the grain boundaries can be healed by the two-step NVT + NpT equilibration. According to Sections 3 and 4, the OPLS-aa force field and the Martini force field are used for pentacene and C_{60}, respectively. These results illustrate the broad applicability of the studied nucleation-equilibration algorithm. We mention that as another variant of the approach, it is possible to generate samples in which only one molecular species exhibits an amorphous structure. This can be implemented, for example, using extended lattice vectors ($s \gg 1$) for the material for which the order is not retained in the equilibration process, as described above.

6. N-DOPED C_{60} FILMS

We finally apply the nucleation-equilibration approach to the case of doped C_{60} films because of the practical importance of doped systems. Indeed, the doping of organic films can significantly improve their conductivity.[42] 2-cyc-DMBI has recently been shown to effectively dope C_{60} films already at small doping concentrations because of a low Coulomb binding energy as an essential molecule-based doping parameter.[43,44] A more detailed analysis of charge transport in doped films requires the construction of dopant-matrix films with controlled morphological variations in their structures.

https://dx.doi.org/10.1021/acs.jctc.0c01196
J. Chem. Theory Comput. 2021, 17, 1266−1275

This can be provided by generalizing the nucleation-equilibration approach for two-component systems presented in the previous section. For small doping concentrations, we assume the matrix material to be polycrystalline. According to the chosen doping concentration, single 2-cyc-DMBI molecules are first placed at random positions. Then, a defined number of C_{60} grain centers is placed at random positions, as well, which is in agreement with the requested average grain size. In both the steps, the overlap criterion based on critical interatomic distances is considered, as described previously. For simplicity, d_{min} = 2.1 Å is used independently of the atom species. Next, the above stepwise grain growth is performed for the C_{60} grains, yielding prototypical n-doped structures. Representative structures with a doping concentration of 1.3 mol % before and after equilibration are depicted in Figure 9.

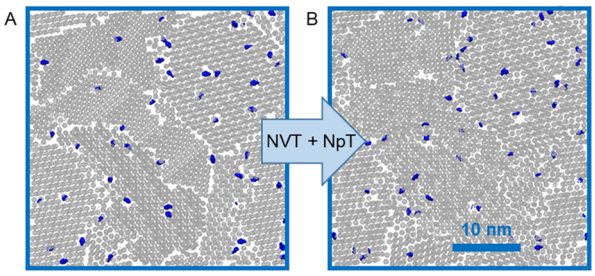

Figure 9. Prototypical n-doped C_{60} structures created by the nucleation algorithm (A) and after full two-step equilibration (B). Doping concentration is 1.3 mol %, and the average size of the C_{60} grains is η = 5000. For clarity, only the first layers are depicted in the viewing direction. System sizes are approximately 37 × 37 × 37 nm^3. Dopants are colored blue.

The resulting structure is a helpful starting point for the systematic theoretical analysis of doped films, including their energetic landscapes and charge-transport properties, both of which are essential to gain further insights into the working principles of the molecular doping of organic films.

7. DISCUSSION AND CONCLUSIONS

The combination of a stochastic nucleation algorithm with an optimized two-step NVT + NpT equilibration approach allows the construction of very large polycrystalline samples with varying morphologies in which both the composition and the degree of the structural order can be independently controlled. Its applications are therefore possible for a large set of model structures, including spherical and nonspherical molecules as well as molecular blends and dilute doped systems. The underlying crystal structure within the grains can be selected, for example, based on experimental data.

The approach was investigated for the face-centered cubic phase of C_{60}, revealing a minimum long-range order of 3.0 nm. In addition, the generalization of the approach was demonstrated for the Holmes phase of pentacene, C_{60}:pentacene blends, and n-doped polycrystalline C_{60} structures. While tested for rigid molecules, the approach can be expected to be similarly applicable to nonrigid molecules because the flexibility does not strongly influence the nucleation step. Moreover, in the equilibration step, the molecular flexibility can be explicitly described by the force field.

The advantages of the approach result from its general applicability because the definition of an environment based on crystal-structure information, the definition of the overlap criterion, and the definition of the aggregation criterion based on empirical probabilities can be performed for a large set of molecules. Along with its low computational effort, this allows its application for samples of experimentally relevant length scales. As demonstrated by Steiner et al. and Vladimirov et al. for 2D polycrystalline structures, such a type of approach can offer essential insights into the influence of polycrystallinity on the electronic energy landscape and the charge transport.[26,45] We believe that the present version of the approach is of particular importance in the vast majority of cases in which a detailed knowledge of the growth mechanism is absent. Furthermore, continued MD simulations on the equilibrated structures with an extended simulation time could be used in future work to study grain-boundary dynamics. Such studies can include further modifications of the structures, for example, the variation of grain shapes or different crystal structures, which can be potentially considered in the input information, allowing for a systematic analysis of a wide range of parameters. While the modeling of specific growth conditions was not in the focus of this work to allow for broad applicability, with more knowledge on the environmental influence on the grain growth and the morphology of specific systems, the algorithm can be refined to mimic specific structures in future studies.

■ ASSOCIATED CONTENT

Supporting Information

The Supporting Information is available free of charge at https://pubs.acs.org/doi/10.1021/acs.jctc.0c01196.

Further information on the correction scheme for small average grain sizes as well as additional Figures (PDF)

■ AUTHOR INFORMATION

Corresponding Author

Frank Ortmann − *Dresden Center for Computational Materials Science and Center for Advancing Electronics Dresden, Technische Universität Dresden, 01062 Dresden, Germany; Department of Chemistry, Technische Universität München, 85748 Garching, Germany;* orcid.org/0000-0002-5884-5749; Email: frank.ortmann@tum.de

Authors

K. Sebastian Schellhammer − *Institute for Materials Science and Max Bergmann Center of Biomaterials, Technische Universität Dresden, 01062 Dresden, Germany; Dresden Center for Computational Materials Science and Center for Advancing Electronics Dresden, Technische Universität Dresden, 01062 Dresden, Germany;* orcid.org/0000-0001-8418-6401

Gianaurelio Cuniberti − *Institute for Materials Science and Max Bergmann Center of Biomaterials, Technische Universität Dresden, 01062 Dresden, Germany; Dresden Center for Computational Materials Science and Center for Advancing Electronics Dresden, Technische Universität Dresden, 01062 Dresden, Germany;* orcid.org/0000-0002-6574-7848

Complete contact information is available at: https://pubs.acs.org/10.1021/acs.jctc.0c01196

Notes

The authors declare no competing financial interest.

https://dx.doi.org/10.1021/acs.jctc.0c01196
J. Chem. Theory Comput. 2021, 17, 1266−1275

■ ACKNOWLEDGMENTS

We gratefully acknowledge support from the German Excellence Initiative via the Cluster of Excellence EXC 1056 "Center for Advancing Electronics Dresden" (cfAED). F.O. would like to thank the Deutsche Forschungsgemeinschaft for the financial support (grant OR 349/1-1 and OR 349/3-1). Computational resources were provided by the Center for Information Services and High Performance Computing (ZIH) of the Dresden University of Technology.

■ ABBREVIATIONS

COM, center of mass; MD, molecular dynamics; PDF, pair-distribution function.

■ REFERENCES

(1) Meyer zu Heringdorf, F.-J.; Reuter, M. C.; Tromp, R. M. Growth Dynamics of Pentacene Thin Films. *Nature* **2001**, *412*, 517−520.
(2) Jin, Q.; Li, D.; Qi, Q.; Zhang, Y.; He, J.; Jiang, C. Two-Step Growth of Large Pentacene Single Crystals Based on Crystallization of Pentacene Monolayer Film. *Cryst. Growth Des.* **2012**, *12*, 5432−5438.
(3) Shtein, M.; Mapel, J.; Benziger, J. B.; Forrest, S. R. Effects of Film Morphology and Gate Dielectric Surface Preparation on the Electrical Characteristics of Organic-Vapor-Phase-Deposited Pentacene Thin-Film Transistors. *Appl. Phys. Lett.* **2002**, *81*, 268−270.
(4) Stadlober, B.; Satzinger, V.; Maresch, H.; Somitsch, D.; Haase, A.; Pichler, H.; Rom, W.; Jakopic, G. Structural and Electrical Properties of Polymorphic Pentacene Thin Films. *In Organic Field Effect Transistors II*; Dimitrakopoulos, C. D., Ed.; SPIE, 2003; Vol. *5217*, 112.
(5) Cheng, H. L.; Mai, Y. S.; Chou, W. Y.; Chang, L. R.; Liang, X. W. Thickness-Dependent Structural Evolutions and Growth Models in Relation to Carrier Transport Properties in Polycrystalline Pentacene Thin Films. *Adv. Funct. Mater.* **2007**, *17*, 3639−3649.
(6) Sato, N.; Seki, K.; Inokuchi, H.; Harada, Y. Photoemission from an Amorphous Pentacene Film. *Chem. Phys.* **1986**, *109*, 157−162.
(7) Choo, M. H.; Kim, J. H.; Im, S. Hole Transport in Amorphous-Crystalline-Mixed and Amorphous Pentacene Thin-Film Transistors. *Appl. Phys. Lett.* **2002**, *81*, 4640−4642.
(8) Rivnay, J.; Jimison, L. H.; Northrup, J. E.; Toney, M. F.; Noriega, R.; Lu, S.; Marks, T. J.; Facchetti, A.; Salleo, A. Large Modulation of Carrier Transport by Grain-Boundary Molecular Packing and Microstructure in Organic Thin Films. *Nat. Mater.* **2009**, *8*, 952−958.
(9) Schweicher, G.; Olivier, Y.; Lemaur, V.; Geerts, Y. H. What Currently Limits Charge Carrier Mobility in Crystals of Molecular Semiconductors? *Isr. J. Chem.* **2014**, *54*, 595−620.
(10) Huang, Y.; Kramer, E. J.; Heeger, A. J.; Bazan, G. C. Bulk Heterojunction Solar Cells: Morphology and Performance Relationships. *Chem. Rev.* **2014**, *114*, 7006−7043.
(11) Jao, M.-H.; Liao, H.-C.; Su, W.-F. Achieving a High Fill Factor for Organic Solar Cells. *J. Mater. Chem. A* **2016**, *4*, 5784−5801.
(12) Park, J. W.; Lee, K.; Choi, Y.-S.; Kim, J.-H.; Jeong, D.; Kwon, Y.-N.; Park, J.-B.; Ahn, H. Y.; Park, J.-I.; Lee, H. S.; et al. The Prediction of Hole Mobility in Organic Semiconductors and Its Calibration Based on the Grain-Boundary Effect. *Phys. Chem. Chem. Phys.* **2016**, *18*, 21371−21380.
(13) Landi, A.; Troisi, A.; Peluso, A. Explaining Different Experimental Hole Mobilities: Influence of Polymorphism on Dynamic Disorder in Pentacene. *J. Mater. Chem. C* **2019**, *7*, 9665−9670.
(14) Coropceanu, V.; Cornil, J.; da Silva Filho, D. A.; Olivier, Y.; Silbey, R.; Brédas, J.-L.. Charge Transport in Organic Semiconductors. 2007.
(15) Ortmann, F.; Roche, S. Polaron Transport in Organic Crystals: Temperature Tuning of Disorder Effects. *Phys. Rev. B* **2011**, *84*, 180302.
(16) Gollub, C.; Avdoshenko, S.; Gutierrez, R.; Berlin, Y.; Cuniberti, G. Charge Migration in Organic Materials: Can Propagating Charges Affect the Key Physical Quantities Controlling Their Motion? *Isr. J. Chem.* **2012**, *52*, 452−460.
(17) Elschner, C.; Schrader, M.; Fitzner, R.; Levin, A. A.; Bäuerle, P.; Andrienko, D.; Leo, K.; Riede, M. Molecular Ordering and Charge Transport in a Dicyanovinyl-Substituted Quaterthiophene Thin Film. *RSC Adv.* **2013**, *3*, 12117.
(18) Radke, K. S.; Scholz, R.; Ortmann, F.; Leo, K.; Cuniberti, G. Dynamic Effects on the Charge Transport in an Organic Near-Infrared Absorber Material. *J. Phys. Chem. C* **2014**, *118*, 6537−6547.
(19) Ortmann, F.; Radke, K. S.; Günther, A.; Kasemann, D.; Leo, K.; Cuniberti, G. Materials Meets Concepts in Molecule-Based Electronics. *Adv. Funct. Mater.* **2015**, *25*, 1933−1954.
(20) Giannini, S.; Carof, A.; Ellis, M.; Yang, H.; Ziogos, O. G.; Ghosh, S.; Blumberger, J. Quantum Localization and Delocalization of Charge Carriers in Organic Semiconducting Crystals. *Nat. Commun.* **2019**, *10*, 1−12.
(21) Yavuz, I.; Martin, B. N.; Park, J.; Houk, K. N. Theoretical Study of the Molecular Ordering, Paracrystallinity, And Charge Mobilities of Oligomers in Different Crystalline Phases. *J. Am. Chem. Soc.* **2015**, *137*, 2856−2866.
(22) Schrader, M.; Körner, C.; Elschner, C.; Andrienko, D. Charge Transport in Amorphous and Smectic Mesophases of Dicyanovinyl-Substituted Oligothiophenes. *J. Mater. Chem.* **2012**, *22*, 22258.
(23) Baumeier, B.; Stenzel, O.; Poelking, C.; Andrienko, D.; Schmidt, V. Stochastic Modeling of Molecular Charge Transport Networks. *Phys. Rev. B* **2012**, *86*, 184202.
(24) Evans, D. R.; Kwak, H. S.; Giesen, D. J.; Goldberg, A.; Halls, M. D.; Oh-e, M. Estimation of Charge Carrier Mobility in Amorphous Organic Materials Using Percolation Corrected Random-Walk Model. *Org. Electron.* **2016**, *29*, 50−56.
(25) Kwiatkowski, J. J.; Frost, J. M.; Nelson, J. The Effect of Morphology on Electron Field-Effect Mobility in Disordered C60 Thin Films. *Nano Lett.* **2009**, *9*, 1085−1090.
(26) Steiner, F.; Poelking, C.; Niedzialek, D.; Andrienko, D.; Nelson, J. Influence of Orientation Mismatch on Charge Transport across Grain Boundaries in Tri-Isopropylsilylethynyl (TIPS) Pentacene Thin Films. *Phys. Chem. Chem. Phys.* **2017**, *19*, 10854−10862.
(27) Nosé, S. A Unified Formulation of the Constant Temperature Molecular Dynamics Methods. *J. Chem. Phys.* **1984**, *81*, 511−519.
(28) Hoover, W. G. Canonical Dynamics: Equilibrium Phase-Space Distributions. *Phys. Rev. A* **1985**, *31*, 1695−1697.
(29) Berendsen, H. J. C.; Postma, J. P. M.; van Gunsteren, W. F.; DiNola, A.; Haak, J. R. Molecular Dynamics with Coupling to an External Bath. *J. Chem. Phys.* **1984**, *81*, 3684−3690.
(30) Abraham, M. J.; Murtola, T.; Schulz, R.; Páll, S.; Smith, J. C.; Hess, B.; Lindahl, E. GROMACS: High Performance Molecular Simulations through Multi-Level Parallelism from Laptops to Supercomputers. *Software X* **2015**, *1-2*, 19−25.
(31) Páll, S.; Abraham, M. J.; Kutzner, C.; Hess, B.; Lindahl, E. *Tackling Exascale Software Challenges in Molecular Dynamics Simulations with GROMACS*; Springer, Cham, 2015; 3−27.
(32) Wennberg, C. L.; Murtola, T.; Páll, S.; Abraham, M. J.; Hess, B.; Lindahl, E. Direct-Space Corrections Enable Fast and Accurate Lorentz−Berthelot Combination Rule Lennard-Jones Lattice Summation. *J. Chem. Theory Comput.* **2015**, *11*, 5737−5746.
(33) Heiney, P. A.; Fischer, J. E.; McGhie, A. R.; Romanow, W. J.; Denenstein, A. M.; McCauley, J. P., Jr.; Smith, A. B.; Cox, D. E. Orientational Ordering Transition in Solid C 60. *Phys. Rev. Lett.* **1991**, *66*, 2911−2914.
(34) David, W. I. F.; Ibberson, R. M.; Dennis, T. J. S.; Hare, J. P.; Prassides, K. Structural Phase Transitions in the Fullerene C_{60}. *Europhys. Lett.* **1992**, *18*, 735−736.
(35) Monticelli, L. On Atomistic and Coarse-Grained Models for C_{60} Fullerene. *J. Chem. Theory Comput.* **2012**, *8*, 1370−1378.
(36) Girifalco, L. A. Interaction Potential for Carbon (C60) Molecules. *J. Phys. Chem.* **1991**, *95*, 5370−5371.

https://dx.doi.org/10.1021/acs.jctc.0c01196
J. Chem. Theory Comput. 2021, 17, 1266−1275

(37) Girifalco, L. A. Molecular Properties of Fullerene in the Gas and Solid Phases. *J. Phys. Chem.* **1992**, *96*, 858−861.
(38) Holmes, D.; Kumaraswamy, S.; Matzger, A. J.; Vollhardt, K. P. C. On the Nature of Nonplanarity in the [N]Phenylenes. *Chem. - A Eur J.* **1999**, *5*, 3399−3412.
(39) Jorgensen, W. L.; Tirado-Rives, J. The OPLS [Optimized Potentials for Liquid Simulations] Potential Functions for Proteins, Energy Minimizations for Crystals of Cyclic Peptides and Crambin. *J. Am. Chem. Soc.* **1988**, *110*, 1657−1666.
(40) William, L. J.; Maxwell, D. S.; Tirado-Rives, J. Development and Testing of the OPLS All-Atom Force Field on Conformational Energetics and Properties of Organic Liquids. *J. Am. Chem. Soc.* **1996**, *118*, 11225−11236.
(41) Drummy, L. F.; Kübel, C.; Lee, D.; White, A.; Martin, D. C. Direct Imaging of Defect Structures in Pentacene Nanocrystals. *Adv. Mater.* **2002**, *14*, 54−57.
(42) Salzmann, I.; Heimel, G.; Oehzelt, M.; Winkler, S.; Koch, N. Molecular Electrical Doping of Organic Semiconductors: Fundamental Mechanisms and Emerging Dopant Design Rules. *Acc. Chem. Res.* **2016**, *49*, 370−378.
(43) Schwarze, M.; Naab, B. D.; Tietze, M. L.; Scholz, R.; Pahner, P.; Bussolotti, F.; Kera, S.; Kasemann, D.; Bao, Z.; Leo, K. Analyzing the N-Doping Mechanism of an Air-Stable Small-Molecule Precursor. *ACS Appl. Mater. Interfaces* **2017**, *10*, 1340−1346.
(44) Gaul, C.; Hutsch, S.; Schwarze, M.; Schellhammer, K. S.; Bussolotti, F.; Kera, S.; Cuniberti, G.; Leo, K.; Ortmann, F. Insight into Doping Efficiency of Organic Semiconductors from the Analysis of the Density of States in N-Doped C60 and ZnPc. *Nat. Mater.* **2018**, *17*, 439−444.
(45) Vladimirov, I.; Kühn, M.; Geßner, T.; May, F.; Weitz, R. T. Energy Barriers at Grain Boundaries Dominate Charge Carrier Transport in an Electron-Conductive Organic Semiconductor. *Sci. Rep.* **2018**, *8*, 14868.

https://dx.doi.org/10.1021/acs.jctc.0c01196
J. Chem. Theory Comput. 2021, 17, 1266−1275